LBL--33157

DE93 007724

Using Coherent Illumination to Extend HRTEM Resolution: Why We Need a FEG-TEM for HREM

M.A. O'Keefe

Materials Science Division
National Center for Electron Microscopy
Lawrence Berkeley Laboratory
University of California, Berkeley, CA 94720

Microstructures of Materials, Berkeley, CA. 22, 23 Oct. 92

This work was supported in part by the Director, Office of Energy Research, Office of Basic Energy Sciences, Materials Science Division of the U.S. Department of Energy under Contract No. DE-AC03-76SF00098.

Using Coherent Illumination to Extend HRTEM Resolution: Why We Need a FEG-TEM for HREM

Michael A. O'Keefe
National Center for Electron Microscopy
Materials Science Division, Lawrence Berkeley Laboratory
University of California, B72-213
Berkeley, California 94720

Abstract

The resolution of a high-resolution transmission electron microscope (HRTEM) has traditionally been defined in terms of its Scherzer resolution limit at optimum defocus. However, even beyond the Scherzer limit, spatial frequencies can be transferred from the specimen to the image, out to the so-called information limit of the electron microscope. The information limit of the HRTEM is determined by the degree of energy spread in the electron beam used to illuminate the sample. Since a HRTEM equipped with a field-emission gun (FEG) will produce an electron beam of high coherence with little energy spread, it can achieve an improved information-limit, and can thus be used to produce through-focus series of images containing information well beyond its nominal (Scherzer) resolution limit. Suitable computer processing of such series of images can produce composite images at resolutions approaching the microscope information limit. For such a FEG-TEM, combined with suitable computer image processing, resolution can approach 1Å.

I. INTRODUCTION

In 1976, Gareth Thomas (and several others) proposed the establishment of the National Center for Electron Microscopy (NCEM). One function of the NCEM was to provide users with state-of-the-art high resolution electron microscopy, and the method chosen was to install a high-voltage HRTEM designed to NCEM specifications, the JEOL ARM-1000 capable of operating with an electron beam energy of 1MeV. Until recently, the highest resolution microscope in existence, the ARM has a Scherzer resolution limit [1] of 1.3Å and routinely attains resolutions of 1.6Å. In practice its Scherzer resolution is limited to a value determined by its information limit.

To extend HRTEM resolution beyond 1.6Å in the next generation of HRTEMs at the NCEM, one attractive way will be to utilize the high information limit of the FEG-TEM to approach an image resolution limit of 1Å.

For a thin specimen, Scherzer resolution is defined to occur at the highest spatial frequency that can be transferred into the image with the same phase as all lower frequencies. On the other hand, the information limit is defined as the highest spatial frequency that can be transferred with significant amplitude regardless of any phase changes at lower frequencies [2]. With suitable computer processing of a through-focus series of images, any misphased frequencies can be corrected, and an image produced that mimics a Scherzer image, but with a resolution equal to the information limit.

II. RESOLUTION AND INFORMATION LIMIT

For thin specimens the phase-contrast transfer function (commonly called the CTF) maps the transfer of information from the specimen (strictly, the electron wave at the specimen exit surface) into the image over a range of spatial frequencies. Transfer of information at any spatial frequency is largest where the CTF has the largest amplitude (i.e. lies furthest from the horizontal axis). Comparison of the CTF of the ARM with the CTF for a mid-voltage HRTEM (the 400keV 4000EX) demonstrates the difference between the Scherzer resolution and the information limit (figure 1). The CTFs in figure 1 show that transfer for both microscopes exceeds 50% down to spacings of 2Å, then tapers to zero at 1.3Å; the information limit is defined to be the spacing corresponding to the highest frequency at which significant transfer occurs, say 1.4Å in this case. The major difference between the curves is that the 4000EX CTF goes through zero at 1.65Å as it reverses sign from negative (below the axis) to positive. One definition for Scherzer resolution is the spacing at this "crossover" frequency. Note that the mid-voltage HRTEM has an information limit (1.4Å) that is better than its Scherzer resolution (1.65Å), whereas the cross-over value (1.3Å) of the high-voltage ARM is better than the information limit, and is never reached in practice.

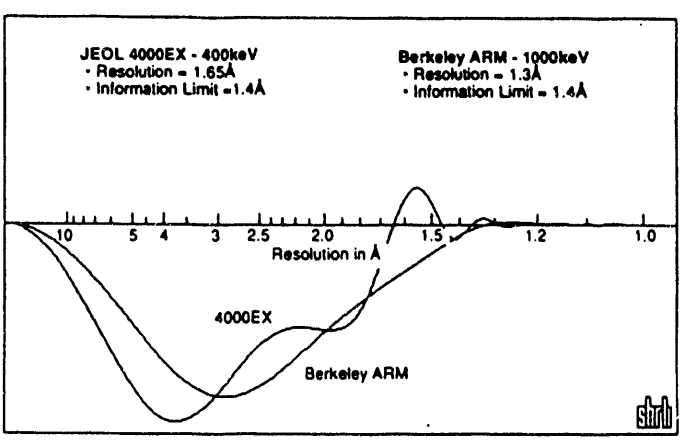

Fig. 1. Phase-contrast transfer functions at optimum defocus for the 1MeV JEOL ARM-1000 and the 400keV 4000EX. Transfer is plotted vertically and spatial frequency horizontally; the (linear) frequency scale is marked (non-linearly) in Å for convenience.

An early illustration of the additional information available in a through-focus series of images dates from the year in which the NCEM was proposed.

Figure 2(a) shows the image obtained at optimum defocus on a JEOL 100B from a thin crystal of the block oxide $Nb_{12}O_{29}$. At this resolution, the large (3.8Å) tunnels through the structure are visible as groups of 2x3 white spots. Figure 2(b) shows an image of the same structure taken with a Hitachi H-1250 at 1MeV; at this resolution (~2.5Å) additional smaller tunnels are visible as smaller white spots lying between the groups of larger spots [3].

Although the 100B was incapable of resolving the small tunnels in a structure image taken at optimum defocus, information about them *was* passed at a higher defocus value. Figure 3 shows a pair of micrographs obtained on the 100B at two defocus values. In the optimum-defocus image (-650Å), the large tunnels are visible but not the small ones. In the image taken at -1600Å, the small tunnels are visible, but the large tunnels are now "scrambled" due to mis-phasing of some of the lower spatial frequencies that define them [4].

Thus it required two micrographs to be taken on the 100B to obtain the same information as is present in one optimum-defocus H-1250 micrograph. By comparing the two 100B micrographs with images simulated using the SHRLI programs [5], the correctness of the crystal structure model used could be verified out to the largest spatial frequency transferred in the second image (fig.3b). However, given the computer software and hardware that is now available (but was not in 1976), the two 100B images of figure 3 could be combined to produce one composite image with a resolution close to that of the H-1250 image of figure 2(b).

Notice that the principal feature of each image in the two-member "though-focus series" of figure 3 has the same phase; the large spots are white at -650Å defocus, and the small spots are white at -1600Å defocus. The features are in phase because the defocus values were specially chosen so that the corresponding CTFs contain large "passbands" of spatial frequencies; the first image was obtained near optimum defocus (-650Å) and the second at a defocus (-1600Å) with a ratio to optimum defocus of $\sqrt{9.5}$ to $\sqrt{1.5}$.

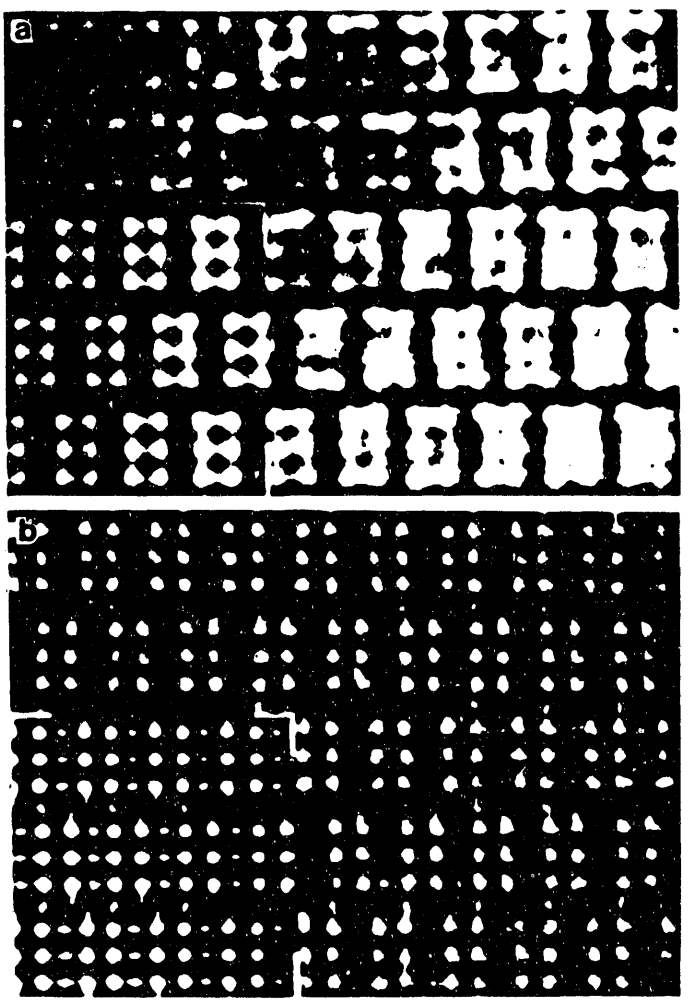

Fig. 2. Structure images of $Nb_{12}O_{29}$ at (a) 100keV with 4Å resolution (S. Iijima), and (b) 1MeV with 2.5Å resolution (S. Horiuchi). The inserts at lower left of each micrograph are SHRLI images computed for a 38Å thick crystal [3].

XBB 848-6142

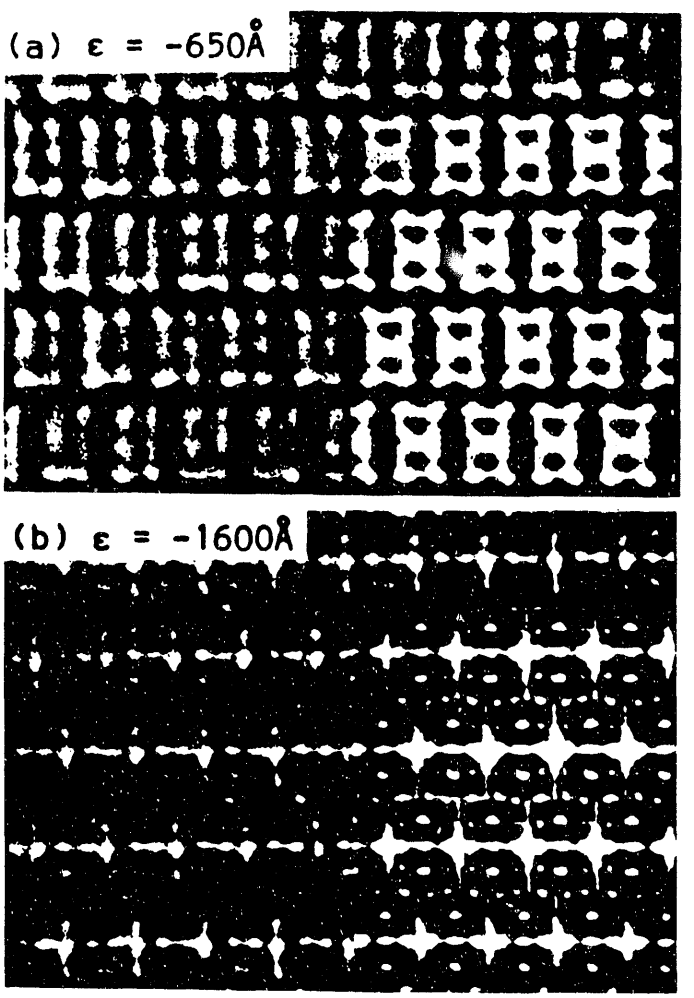

Fig. 3. Images of $Nb_{12}O_{29}$ taken at 100keV (S. Iijima) for defocus values of (a) -650Å, and (b) -1600Å. The inserts at lower right of each micrograph are SHRLI images computed for a 20Å thick crystal [4].

XBB 9211-09096

III. PASSBANDS

By careful comparison of experimental and simulated images of several structures, O'Keefe and Buseck [5] established that the best defocus for maximum resolution in a thin-crystal structure image was $\sqrt{(3C_S\lambda/2)}$, where C_S is the spherical aberration coefficient of the microscope lens and λ is the electron wavelength.

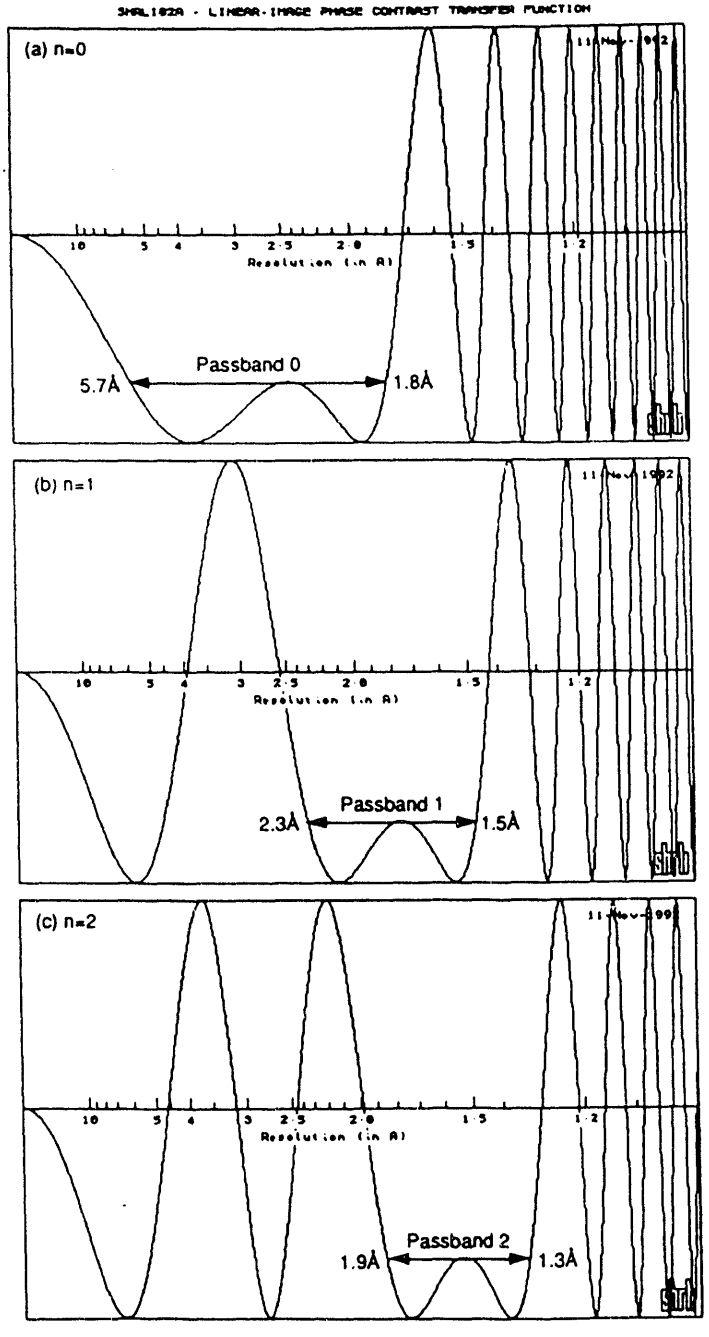

Fig. 4. Phase-contrast transfer functions for a mid-voltage (300keV) electron microscope with a C_S value of 0.7mm, at (a) zeroth-passband (optimum) defocus (n=0 in equation 1), (b) first-passband defocus (n=1), (c) second-passband defocus (n=2). Major passbands are marked at the 70%-transfer level, and cover the ranges (a) 5.7-1.8Å, (b) 2.3-1.5Å, (c) 1.9-1.3Å.

Generalizing to the case of a through-focus series of images, O'Keefe and Buseck [5] proposed obtaining "passband" images by using a series of "optimum" defocus values set at

$$\varepsilon_{opt} = \sqrt{[(8n+3)/2]\, C_S^{1/2}\, \lambda^{1/2}} \qquad (1)$$

where n = 0, 1, 2, 3, ... This set of defocus values produced a series of images with CTFs which contain major passbands within which transfer was better than 70%. In fact the spatial frequencies at the upper and lower limits of the major passbands are just

$$u_{\pm} = \sqrt{\{\sqrt{[(8n+3)/2]} \pm 1\}\, C_S^{-1/4} \lambda^{-3/4}} \qquad (2)$$

Figure 4 shows how the major passbands overlap in spatial frequency, producing a through-focus series that can be processed (a process called focal-series restoration) to produce one image containing all spatial frequencies out to the u_+ value of the highest member of the focal series. As the value of n is increased, the passbands become narrower, but continue to add more information to the image series.

IV. DAMPING ENVELOPES

In addition to the phase changes that are imposed by the objective lens, and described by the CTF curve, transfer of information from the object into the image is also modulated by the effects of partial coherence of the electron beam.

Imperfect spatial coherence occurs because electron waves at different angles within the convergent illuminating beam are not mutually coherent because the electron source has a finite size. The parameter used to model the effect is the semi-angle of convergence α. A good estimate of the value of α can be obtained from the focussed diffraction pattern [6].

Imperfect temporal coherence is manifested as a spread of focus caused by energy spread in the incident electron beam, as well as variations in objective lens current and accelerating voltage. Its effect is modelled with a parameter Δ, the half-width of a Gaussian spread of focus. An estimate of Δ can be obtained by computing

$$\Delta = C_C \sqrt{[(\delta V/V)^2 + (2\delta I/I)^2 + (\delta E/E)^2]} \qquad (3)$$

where C_C is the chromatic aberration coefficient for the objective lens, $\delta V/V$ is the fractional change in voltage over the time scale of image acquisition, $\delta I/I$ is the fractional change in lens current, and $\delta E/E$ is the energy spread in the electron beam as a fraction of the total energy. Also, any vertical vibration of the specimen with respect to the lens will contribute to Δ.

Frank [7] showed that the resolution-limiting results of these coherence effects on information transfer into the image could be described in reciprocal space as "damping envelope" functions that multiply the CTF curves.

The envelope for the incident beam convergence produced by spatial coherence has the form

$$E_\alpha(u) = \exp\{-\pi^2\alpha^2(\varepsilon+\lambda^2 C_S u^2)^2 u^2\} \qquad (4)$$

where ε is defocus and α is the semi-angle of the convergence cone at the specimen surface, and specifies the range of angles (of beam misorientation with respect to the optic axis) over which images are integrated to form the recorded image [6].

The envelope for the spread of focus produced by partial temporal coherence has the form

$$E_\Delta(u) = \exp\{-\tfrac{1}{2}\pi^2\lambda^2\Delta^2u^4\} \qquad (5)$$

where Δ is the halfwidth of a Gaussian spread-of-focus that models the fact that the recorded image is the sum of many images all at slightly different values of focus.

The shapes of the damping envelopes are shown in figure 5 for a number of different values of Δ and α. The envelopes attenuate the higher-frequency bands, limiting the frequency to which information can be transferred; higher values of Δ and α produce more attenuation.

Because the envelope functions slope gradually to zero, it is difficult to assign "cutoff" frequencies beyond which transfer can be considered to be insignificant, especially in the case of the $E_\Delta(u)$ envelope where the slope is very shallow (fig 5b). Conventionally, we set the cutoffs at the frequencies where the envelopes drop to values of exp(-2) or 13.7%. Then the cutoffs for u_α and u_Δ can be written as [8]*

$$u_\Delta = (\pi\lambda\Delta/2)^{-\frac{1}{2}} \quad \text{and} \quad u_\alpha = \sqrt[3]{S_+} + \sqrt[3]{S_-} \qquad (6)$$

where

$$S_\pm = \{3.3/(4\pi\alpha) \pm \sqrt{[\varepsilon^3/(27C_S\lambda^2) + (3.3/(4\pi\alpha))^2]}\}/\{C_S\lambda^2\}$$

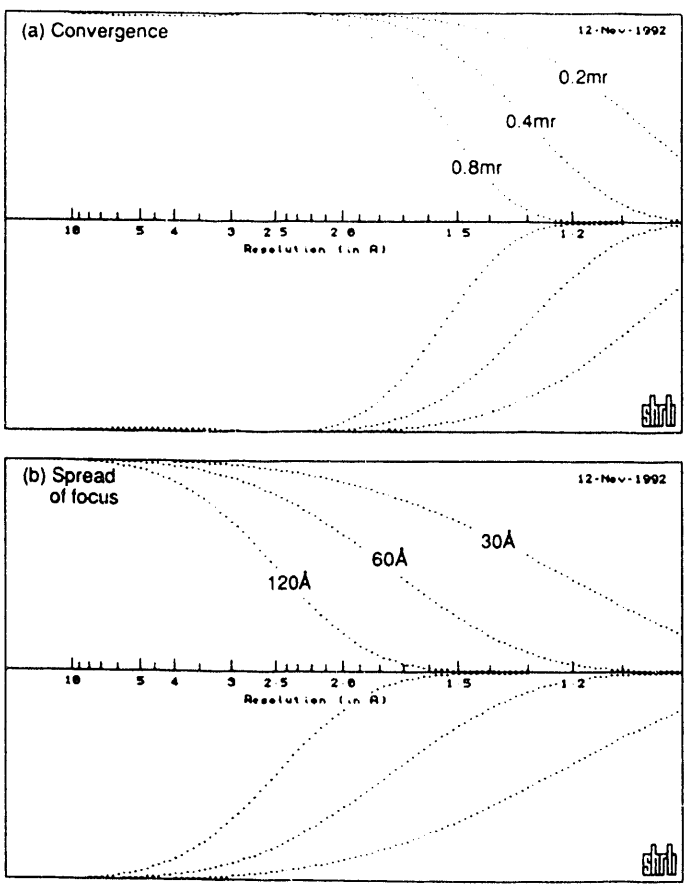

Fig.5. Damping envelope functions for a 300keV microscope with a C_S value of 0.7mm. (a) envelopes for incident beam convergence semi-angles of 0.8, 0.4 and 0.2 milliradians. (b) envelopes for spread of focus values of 120, 60 and 30Å.

* Equations 6 are in the Fortran program HP as the functions LIMD and LIMA; HP is available from the EMSA EMPPDL.

and $S_\pm$ holds only for values of defocus larger (more positive) than $-1.23C_S^{1/3}(\lambda/\alpha)^{2/3}$.

The effect of the convergence envelope E_α on the major passband of a CTF at an optimum defocus is less severe than the effect of E_Δ. Figure 6 compares the effects of an incident beam convergence of 0.8mrad (a) with that of 60Å spread of focus (b). Although the cutoff value for u_α (1.40Å), is slightly more severe than that for u_Δ (1.36Å), the major passband is damped much more strongly by the spread of focus envelope, yet is almost unaffected by convergence.

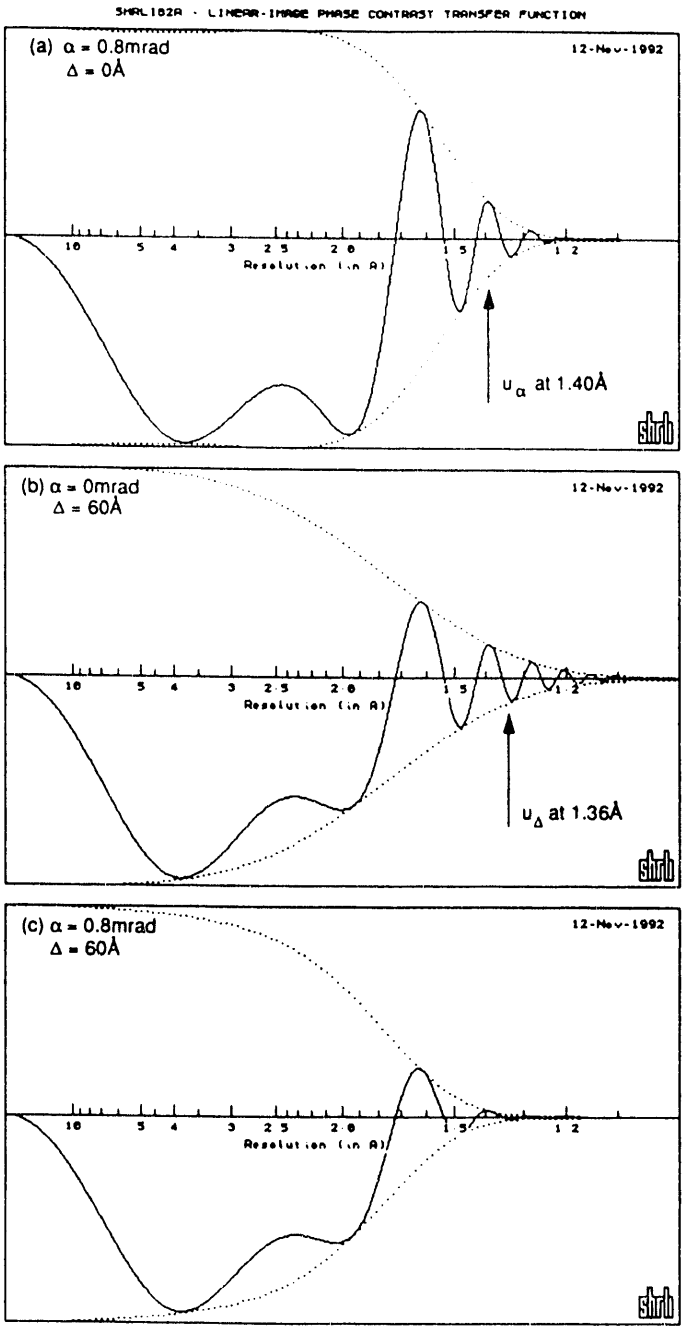

Fig. 6. Optimum-defocus CTFs (solid lines) and damping functions (dotted lines) for a 300keV electron microscope with C_S = 0.7mm. (a) convergence semi-angle α of 0.8mrad. (b) spread-of-focus halfwidth Δ of 80Å. (c) combined effect of the two damping envelopes.

Since the convergence envelope is defocus-dependent, it has only a minor effect on all major passbands. However, spread of focus will damp major-passband-transfer increasingly as defocus is moved further underfocus (i.e. the value of n is increased in equation 1). Thus the information limit is ultimately determined by the spread of focus envelope [2]. Figure 7 shows CTFs calculated with values of α and Δ typical for a HRTEM equipped with a conventional lanthanum hexaboride (LaB_6) filament. Passband 2, with an upper limit of 1.36Å (figure 4), is severely damped by the effect of the spread of focus envelope.

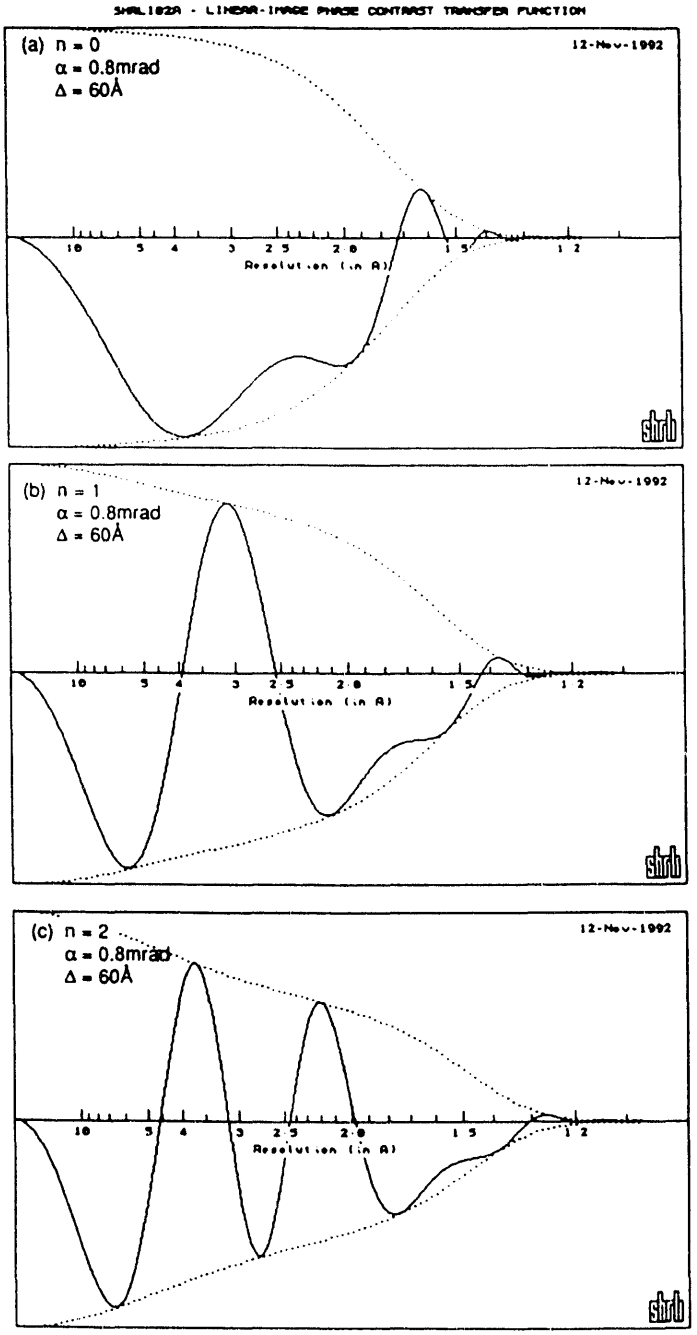

Fig. 7. "LaB_6" CTFs (solid) and damping functions (dotted) at the first three optimum values of defocus, (a) n=0, (b) n=1, and (c) n=2. Spread of focus of 60Å, convergence semiangle of 0.8mrad, voltage of 300kV, and C_S value of 0.7mm.

Because the information limit of the HRTEM is determined by spread of focus, it can only be improved by reducing the value of Δ. From equation (3), such reduction means lowering the values of one or more of the objective lens chromatic aberration coefficient C_C, electron beam energy spread δE, or any lens and voltage variations.

In place of a LaB_6 filament, use of a field-emission gun (FEG) can reduce the value of δE from 1eV down to as low as 0.3eV. Assuming that lens and voltage variations remain at one part per million and the C_C value is 1.5mm, Δ will be almost halved, from 60Å to 36Å . Figure 8 shows

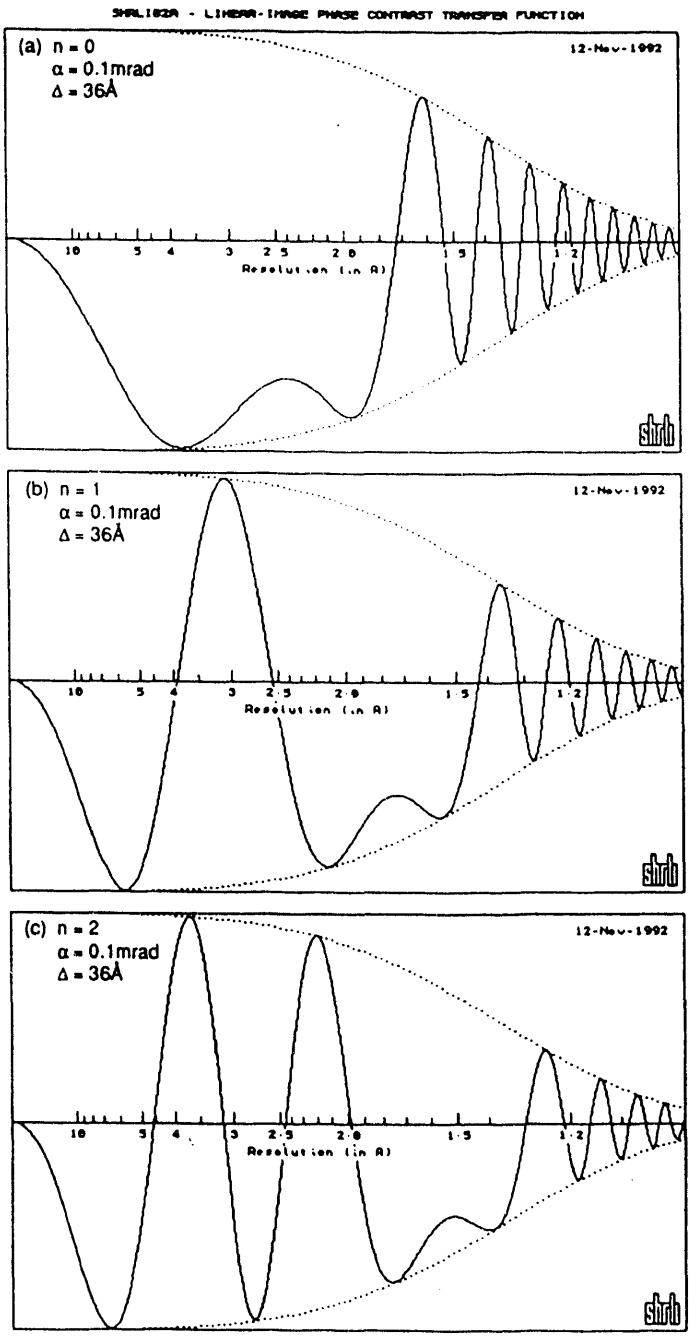

Fig. 8. "FEG" CTFs (solid) and damping functions (dotted) at the first three optimum values of defocus, (a) n=0, (b) n=1, and (c) n=2. Spread of focus of 36Å, convergence semiangle of 0.1mrad, voltage of 300kV, and C_S value of 0.7mm.

CTFs computed for this value of Δ. Compared with the "LaB_6" CTFs of figure 7, the "FEG" CTFs of figure 8 show much improved transfer of spacings below 1.5Å. In particular, although the LaB_6 plots indicate that only three major passbands can be supported, the FEG plots suggest that more major passbands should be achievable. This is borne out by plotting the first three negative-going (and two positive-going) LaB_6 passbands (figure 9a) and comparing the results with plots of the first six negative-going (and five positive-going) FEG CTFs (figure 9b). The plots show how the FEG information limit (1.07Å) is as far beyond the LaB_6 information limit (1.36Å) as the latter is beyond the Scherzer resolution (1.8Å).

VI. CONCLUSIONS

In order to achieve advanced resolution in electron micrographs, the next generation of high-resolution electron microscopes should have improved information limits. With computer processing of suitable focal series of images, images can be produced with resolutions out to these limits. In effect, the image will now have a resolution beyond that of the microscope and limited only by the information limit of the microscope. Currently, improvement of the microscope information limit is best achieved by reducing energy spread in the electron beam, either by use of a field-emission gun or by energy filtering of the high-resolution image.

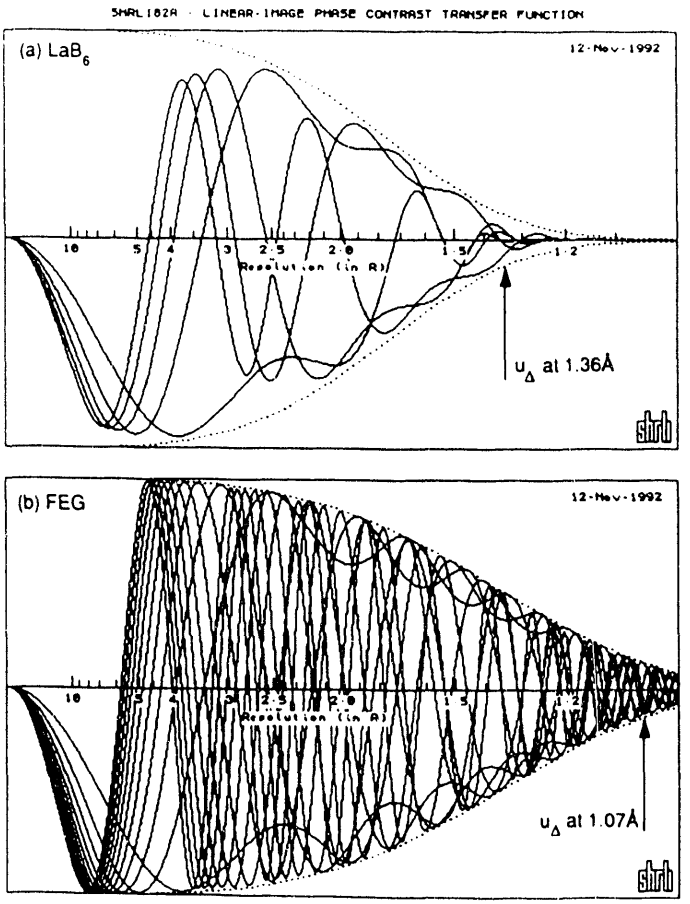

Fig. 9. Comparison of (a) LaB_6 and (b) FEG phase-contrast transfer functions (solid lines) plotted with appropriate values of α and Δ. The dotted lines show the enveloping spread-of-focus damping function, and demonstrate that no transfer can occur beyond this envelope; the information limits of 1.36Å and 1.07Å are marked.

There are several focal series restoration methods capable of producing one micrograph from a through-focus series. These methods range from the linear-image Schiske algorithm [9] to the non-linear procedures of Kirkland [10], the paraboloid method [11], and maximum likelihood [12]. Some of these methods may be more suitable in reliability and speed than others, but all are only as good as the information limit of the electron microscope.

VII. REFERENCES

[1] O. Scherzer, "The theoretical resolution limit of the electron microscope", J. Appl. Phys. 20, pp.20-29, 1949.

[2] M.A. O'Keefe, "Resolution in high-resolution electron microscopy", Ultramicroscopy, accepted, 1992.

[3] R.M. Fisher and T. Imura, "New applications and extensions of the unique advantages of HVEM for physical and materials research", Ultramicroscopy 3, pp.3-18, 1978.

[4] G.R. Anstis and M.A. O'Keefe, "Resolution-limiting effects in electron microscope images", in 34th Ann. Proc. EMSA, Miami Beach, Florida, pp.480-481, 1976.

[5] M.A. O'Keefe and P. R. Buseck, "Computation of high resolution TEM images of minerals", Transactions of the ACA 15, pp.27-46, 1979.

[6] M.A. O'Keefe and J.V. Sanders, "*n*-Beam lattice images. VI. Degradation of image resolution by a combination of incident-beam divergence and spherical aberration", Acta Cryst. A31, pp.307-310, 1975.

[7] J. Frank, "The envelope of electron microscope transfer functions for partially coherent illumination", Optik 38, pp. 519-536, 1973.

[8] M.A. O'Keefe and A.J. Pitt, "The WPO image of $Ti_2Nb_{10}O_{29}$ as a measure of resolution", in Electron Microscopy 1980, Proc. 7th European Cong. on Electron Microscopy, The Hague, Netherlands, 1980, pp.122-123.

[9] P. Schiske, "Image processing using additional statistical information about the object", in Image processing and computer-aided design, Ed. P.W. Hawkes, Acad. Press, London, pp.82-90, 1973.

[10] E.J. Kirkland, "High-resolution image processing of bright-field electron micrographs", in 42nd Ann. Proc. EMSA, Detroit, Michigan, pp. 432-433, 1984.

[11] D. Van Dyck and M. Op de Beeck, "New direct methods for phase and structure retrieval in HRTEM", in Proceedings of the 12th International Congress. for Electron Microscopy, Seattle, Washington, pp. 26-27, 1990.

[12] W. Coene "A practical algorithm for maximum-likelihood HREM image reconstruction", in 50th Ann. Proc. EMSA, Boston, Massachusetts, pp. 986-987, 1992.

END

DATE FILMED

4/19/93